Available online at www.sciencedirect.com

Manufacturing Letters

Manufacturing Letters 33 (2022) 9–16

50th SME North American Manufacturing Research Conference (NAMRC 50, 2022)

Real-time Multiple-particle Tracking in Ultrasonic Spray Pyrolysis

Cade Albert[a], Lin Liu[a*], John Haug[b], Huixuan Wu[b], Ruichen He[c], Jiarong Hong[c]

[a]*Department of Mechanical Engineering, University of Kansas, Lawrence, KS 66049, USA*
[b]*Department of Aerospace Engineering, University of Kansas, Lawrence, KS 66049, USA*
[c]*Department of Mechanical Engineering, University of Minnesota, Minneapolis, MN 55455, USA*

* Corresponding author. Tel.: +1-785-864-1612; fax: +1-785-864-5251. E-mail address: linliu@ku.edu

Abstract

Solid polymer electrolytes (SPEs) hold the potential to revolutionize energy storage by enabling secondary batteries containing lithium metal anodes, which have an ultra-high theoretical capacity of 3860 mAh g^{-1}, compared to a typical graphite anode's theoretical capacity of 372 mAh g^{-1}. The bulk of SPE research focuses on optimizing SPE chemistry, while the manufacturing process receives little attention. In this interdisciplinary study, an electric-field-assisted ultrasonic spray pyrolysis (EFAUSP) setup is proposed and integrated with a cyclone-separator, which was simulated ANSYS Fluent, then built based on the results. Digital in-line holography is performed to determine the droplet size distribution and investigate the droplet trajectories near the substrate surface. This newly proposed EFAUSP setup is based on a 3D printer controller, promising macrostructure and microstructure control in future work. Future work will build upon these results to investigate the mechanical and electrochemical properties of the deposited SPEs.

Keywords: Digital in-line holography; Solid polymer electrolytes; Simulation; Spray Pyrolysis

1. Introduction

Lithium-ion batteries (LIBs), accelerated the wireless revolution, but growing environmental concerns and renewed interest in electric vehicles (EVs) necessitate batteries with greater energy densities than standard LIBs can deliver [1-9]. Lithium metal batteries (LMBs) utilize a Li metal anode with an ultra-high theoretical capacity of 3860 mAh g^{-1} (vs. the 372 mAh g^{-1} theoretical capacity of graphite anodes) [10-14]. LMBs proceeded Sony's 1991 commercialization of the LIB, however, the anode tends to form dendritic lithium (Li) growths that can puncture the separator and short circuit the cell, leading to thermal runaway and explosions [15]. Over the past 40 years, considerable research has been dedicated to realizing solid-state electrolytes (SSEs) to overcome the hurdles faced by LMBs and tap the theoretical capacity of the Li metal anode [1, 7, 16-19]. The solid nature of SSEs permits the use of Li metal anodes by mechanically blocking Li dendrites [20]. SSEs are also non-flammable, unlike organic electrolytes used in most LIBs. Additive manufacturing (AM) applied to Li batteries allows control of both the macrostructure and microstructure for improved battery performance [21]. In 1973, the first ion-conducting polymer, Poly(ethylene oxide) (PEO), was discovered [1, 19]. It is one of the most extensively researched SPEs because it dissolves Li salts and can serve as a backbone for other cross-linked polymers [16, 17, 19, 22-25]. At room temperature, about 60% of a bulk amount of PEO is in the semi-crystalline phase, while the remainder is in the amorphous elastomeric phase, which strongly favors segmental motion and efficient ion transport [17, 18]. The addition of nanoscale ceramic particles as filler disrupts the PEO's crystallinity, thus increasing ionic conductivity. This method has been shown to have a host of benefits ranging from greater mechanical strength to larger voltage stability windows [17, 22, 26-28]. The addition of ceramic nanoparticles, such as silicon dioxide (SiO_2), to PEO yields a nanocomposite solid-state electrolyte (CSSE).

2213-8463 2022 © 2019 The Authors, Published by Elsevier B.V.
Peer review under the responsibility of the scientific committee of NAMRI/SME

SPE or CSSE films are typically prepared separately from the rest of the battery cell (e.g., solvent casting, spin coating, electrospinning) [15, 29, 30]. Creating the SSE independently from the rest of the cell increases interfacial resistance between the electrodes and electrolyte that could be avoided if the SSE was synthesized directly on the electrode. Spray pyrolysis (SP) is an AM technique, commonly used to create thin films, that can be performed in normal room atmosphere without vacuum equipment and is used in numerous industries because it is simple and cost-effective [8, 9, 31-40]. SP encompasses a wide variety of derivatives that share three primary steps described by Perednis and Gauckler: (1) atomization of the precursor solution, (2) transportation of the resultant aerosol, and (3) decomposition of the precursor onto the substrate [38]. Spray pyrolysis is characterized by how the droplets react above the substrate and differs based on substrate temperature. Possible outcomes are shown in Figure 1: (1) the droplet wets the substrate; (2) the droplet evaporates above the substrate such that the precipitate strikes the surface; (3) the droplet evaporates, then the precipitate sublimates, leaving the vapor to undergo a separate reaction on the substrate surface; and (4) all previous steps occur higher above the substrate such that the resulting sublimated vapor undergoes a chemical reaction above the substrate [9, 38, 39]. Decreasing the initial droplet size, while maintaining a constant substrate temperature, has the same effect as raising the substrate temperature, as shown in Figure 1 (b).

The droplet formation method commonly differentiates spray pyrolysis techniques (SPTs) from each other. In ultrasonic spray pyrolysis (USP), an ultrasonic nozzle, or nebulizer, generates droplets by vibrating longitudinally at high frequencies via piezoelectric transducers such that a standing wave forms in the thin film of liquid at the nozzle's tip; these capillary waves then extend off the nozzle tip until they separate from this tip as evenly distributed small droplets [41]. USP distinguishes itself from other atomization techniques by virtue of energy efficiency, low initial droplet velocity and small, narrow, droplet size distribution [13, 14, 41-43]. The Lang equation describes the relationship between ultrasonic frequency and aerosol droplet size [9, 44]:

$$D_{droplet} = 0.34\left(\frac{8\pi\gamma}{\rho f^2}\right)^{1/3} \quad (1)$$

where $D_{droplet}$ is the mean diameter of the droplets, γ is the precursor solution surface tension, ρ is the precursor solution density and f is the frequency of the ultrasound.

In ultrasound-modulated two-fluid (UMTF) atomization, a carrier gas flows around the nozzle tip and causes the capillary waves to collapse into droplets [8, 41]. EFAUSP builds upon ultrasonic spray pyrolysis with the addition of an electric field in the space between the exit of the tubular reactor and the substrate surface. The electric field enables greater surface adhesion, which reduces wasted material and produces a denser, more cohesive, film [35]. In EFAUSP, because the droplets impact the target at low speed in the wet regime, polymer can flow into the pores. As a result, a more uniform coating can be obtained than through pneumatic spray coating [45].

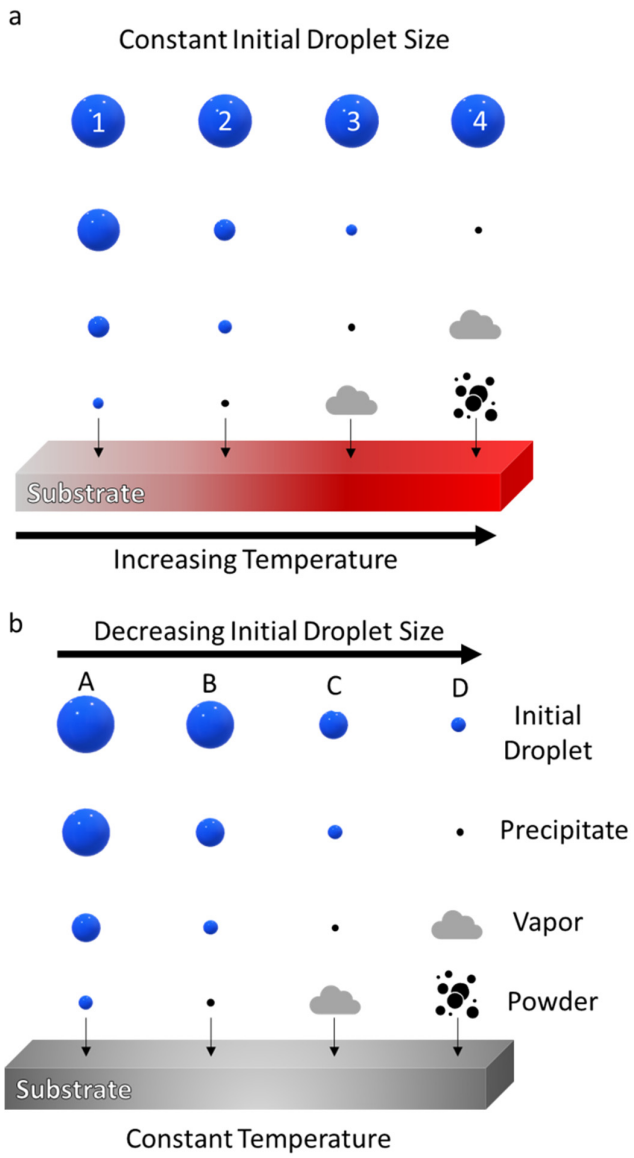

Fig. 1 (a) Description of the deposition processes with increasing substrate temperature; (b) with decreasing initial droplet size

Thin, uniform films are crucial for minimizing interfacial resistance and facilitating uniform current densities over the electrode surfaces. Small droplet size minimizes the coffee ring effect (nonuniform droplet deposits with raised edges at the outer diameter) and facilitates greater control over the microstructure. Though ultrasonic nebulizers have a finer droplet distribution than ultrasonic nozzles, both have droplet distributions far superior to pneumatic atomization. Even though ultrasonic nebulizers have the smallest droplet size and distribution of the methods discussed, nebulizers suffer from low throughput compared to ultrasonic nozzles. As one of the first attempts, we introduce the design of a cyclone separator in the EFAUSP. Since the turbulent jet with sprays possesses a series of eddies that determine the distribution of deposition droplets or particles and, eventually, deposition pattern. A

cyclone separator can utilize the turbulent jet to reduce the number of larger diameter droplets used to form the SPE film while leveraging the throughput advantage of ultrasonic nozzles over nebulizers.

Cyclone separators, or inertial separators, possess a wide variety of configurations and are most commonly used to separate dust particles from an inlet gas stream [46-49]. Compact designs have found use in the pharmaceutical industry, and energy storage research, for the synthesis of submicron-sized particles [50, 51]. Cyclone separators function under the principle that larger particles have greater mass and therefore greater inertia. Thus, the larger particles will tend towards to the outside of the separator and be carried down for collection as waste, while the smaller particles escape upwards on a central upward vortex that spins counter to the outer gas flow. The smaller particles escaping with the outlet gas are typically viewed as inefficiencies, but in the context of SP, this can be leveraged to select droplets of a specific size distribution. Smaller particles are advantageous for SP because small particles evaporate at lower temperatures and have a lower evaporation rate, which results in dense solid films [9]. Thus, such a separator was simulated in ANSYS Fluent 19.1, and is discussed in Section 2.

Nomenclature	
AM	Additive manufacturing
CSSE	Nanocomposite solid-state electrolyte
ρ	Density of precursor solution
$D_{droplet}$	Droplet diameter
EFAUSP	Electric-field-assisted ultrasonic spray pyrolysis
EV	Electric vehicle
f	Frequency of the ultrasound
Li	Lithium
LiTFSI	Lithium-bis(trifluoromethane) sulfonimide
LIB	Lithium-ion battery
LMB	Lithium metal battery
PEO	Poly(ethylene oxide)
SiO_2	Silicon dioxide
SP	Spray pyrolysis
SPE	Solid polymer electrolyte
SPT	Spray pyrolysis technique
SSE	Solid-state electrolyte
γ	Surface tension of precursor solution
UMTF	Ultrasound-modulated two-fluid
USP	Ultrasonic spray pyrolysis

2. ANSYS Fluent Results

A simulation was constructed in ANSYS Fluent 19.1 containing around 550 thousand tetrahedral meshed elements, which used the renormalization group (RNG) k-ε viscous model, which considers the effects of rotation in the closing equations of turbulence. The CFD modeling software ANSYS Fluent considers that when using RNG k-ε to model swirling flows, the effective turbulent viscosity is calculated based on the rotational tensor, a swirl factor, and the turbulent viscosity, and is considered a two-equation model, where turbulent kinetic energy and the dissipation rate of energy are modeled and elaborated in [52]. The simulation was performed on DELL workstation (Precision T3600). Discrete phase modeling was used to simulate the droplets behavior in an applied argon gas flow. Argon gas was being chosen to simulate the dry environment needed for handling lithium salts. Various cyclone separator geometries were simulated, and it was determined that more traditional geometries were too efficient at removing particles from the argon flow and made integrating the ultrasonic nozzle difficult. Thus, a configuration with the nozzle mounted on the top of the separator was chosen. The carrier gas inlet is near the bottom of the separator, and the outlet centerline is positioned slightly below the nozzle tip. The walls of the chamber were set to trap the drops, and the outlet was an escape. The geometry and particle tracks are shown in Figure 2.

a)

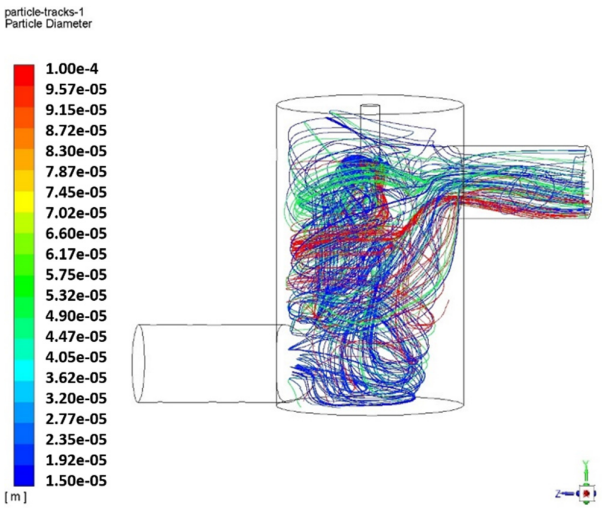

b)

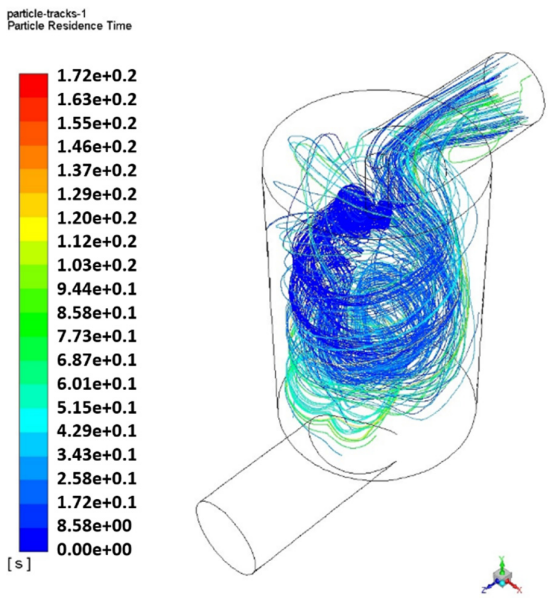

Fig. 2. (a) Particle tracks by particle diameter from ANSYS Fluent 19.1; (b) particle residence time

Based on the simulation 21% of the 100 µm droplets escaped, while 70% were trapped. 78% of the 50 µm droplets escaped. 60% of the 23 droplets escaped and 55% of the 15 µm droplets escaped.

3. Experimental Setup

The experimental setup is broken up into two sections, the EFAUSP setup and the particle-based diagnostic system applied to the EFAUSP setup.

3.1. Electric-Field-Augmented Ultrasonic Spray Pyrolysis

The Electric-Field-Augmented Ultrasonic Spray Pyrolysis (EAUSP) setup is shown in Figure 3. The ultrasonic nozzle used is a 130 kHz wide spray model from Sonaer Inc. The closed-loop filtration glovebox was produced by CLEATECH, LLC. The tubular reactor heater and temperature controller were made by BriskHeat®.

a)

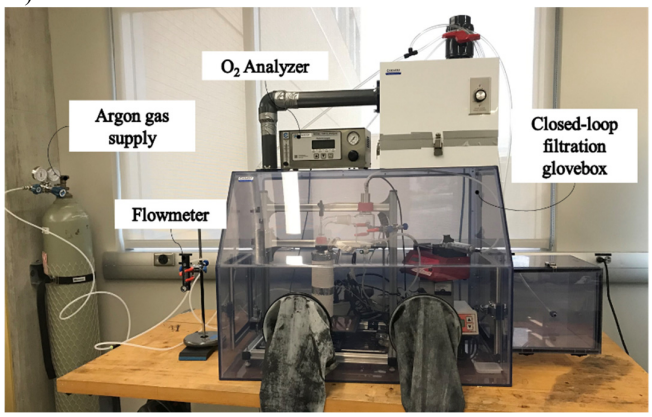

b)

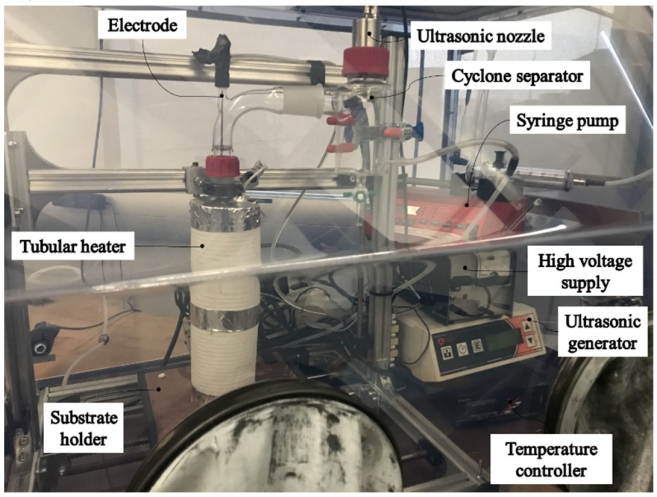

Fig. 3 (a) EFAUSP setup; (b) closeup of EFAUSP setup.

3.2. Precursor Solution Preparation

The viscosity of the precursor solution is the principle limiting factor of ultrasonic atomization. PEO is water soluble but choosing water as the sole solvent does not allow the enough time for solvent evaporation during its short residence time in the tubular reactor. It was experimentally determined that 60% ethanol and 40% distilled water, by volume, was the ideal balance between solubility and evaporation time. Pure ethanal (Decon Labs, Inc.) and lab purity distilled water were. The solutes were SiO_2 nanoparticles particles, 5-20 nm diameter, 60.08 g/mol, (Sigma-Aldrich) and PEO with an average molecular weight 600,000 g/mol (Sigma-Aldrich). The ratio of solutes used was based of 5% weight SiO_2. The molarity was 0.001 mols of solute per liter of solvent. The mixture was stirred rigorously and heated below the boiling point of ethanol until the solutes completely dissolved and the nanoparticles ceased amalgamation.

3.3. Particle-based flow diagnostic system

The particle size out of the ultrasonic nozzle is measured using digital in-line holography (DIH). DIH has emerged recently as a low-cost and highly compact tool for 3D imaging. It employs a coherent light beam to illuminate the sample, and collects the signal (i.e., hologram) generated from the interference of the sample scattered light and the non-scattered portion of the illumination. The 3D position and size of the sample can be subsequently obtained from the hologram through a digital reconstruction process based on light diffraction formulation [53]. Shown in Figure 4 is the ultrasonic spray device used to produce droplet particles. In our test, a He-Ne 632 nm laser is used as the light source and a NAC HX-7 high-speed camera is used to record image at a frame rate of 2000 frames-per-second (fps). The coherent laser beam (reference beam) illuminates the particles in the sample volume, which then reach the camera sensor. The light scattered from particles in the measurement domain also reach the sensor.

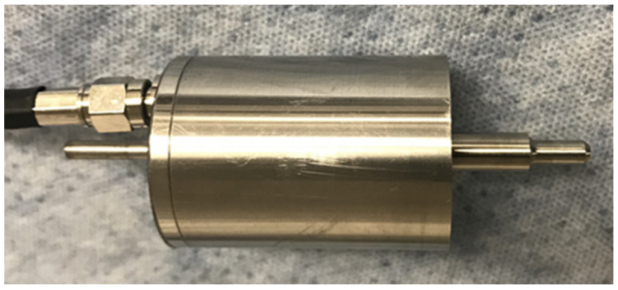

Fig. 4. Ultrasonic Nozzle.

As shown in Figure 5, the interference between the scattered light and undisturbed reference beam results in fringe patterns, which the camera can record. The image usually contains little or no in-focus objects. However, the fringe pattern contains information of both particle shape and location. Thus, the images can be used to digitally reconstruct the 3D position of particles and to measure their diameters. Note that holographic reconstruction contains larger error in the axial direction; however, this does not affect the diameter measurement of spherical particles, as the scale in the other two dimensions can be accurately obtained. The DIH reconstruction includes image enhancement, kernel-based reconstruction, particle/object

segmentation, and post-processing. Recent development allows separate treatment of particles in different size groups [54, 55].

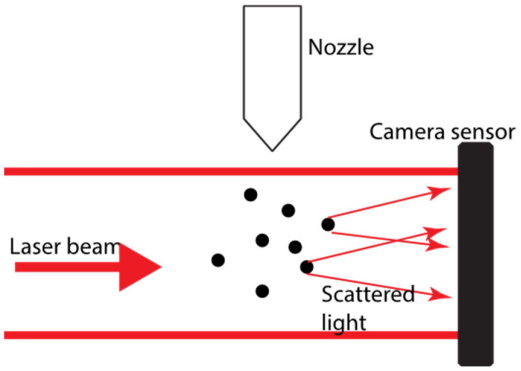

Fig. 5. Sketch of in-line holography setup.

In principle, the holographic result can be used to track the motion of spray particles. However, the DIH field of view is relative small. Hence, in this study, we used direct imaging (normal photography) to observe the spray particle motion above the substrate. A high-repetition-rate ND:YLF laser is expended to a 2D sheet, illuminating the center plane of the jet. The HX-7 camera is place normal to the laser plane, which forms a typical 2D particle imaging system. Figure 6 is a sample image showing the particle distribution above the stagnation point on the substrate. The pulsed laser and camera are synchronized at a framerate of 2000 fps. A sequence of images captures the motion of spray particles in the illuminated plane. Based on the video, we identify the particle position in each image and reconstruct their trajectory. There are many 2D particle-tracking algorithms. The nearest neighbor method was used to start searching for a trajectory at the beginning, and then a switch was made to the minimum acceleration method to identify the following trajectory.

a)

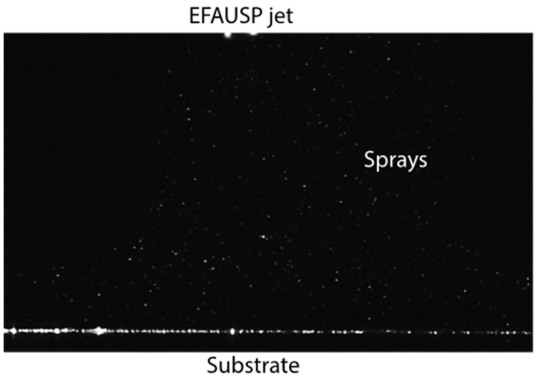

b)

Fig. 6 (a) Sample image of particles above the substrate from high-speed camera; (b) sample photograph of illuminated particles

4. Results and Discussion

The optical measurements provide two main results: 1) the PEO precursor solution droplet size distribution directly from the ultrasonic nozzle, and 2) the spray particle motion above the substrate. The droplet size downstream the cyclone separator is estimated to be smaller than 50 µm.

4.1. PEO solution droplet size distribution

From the data shown in Figure 7, the average diameter was 40 µm with a standard deviation of 18 µm. The probability for a particle to be larger than 40 µm was about 0.3. In other words, the spray contains many tiny droplets and few big particles. However, this spray was directly from the ultrasonic nozzle, and was thus unfiltered. Through a cyclone separator, the larger particles can be captured, which will leave only small particles entering the heating chamber. The filtering process is critical for removing the scattered large droplets and achieving uniform deposited electrolytes. In addition, large droplets may also introduce unnecessary local disturbance in the multiphase flow.

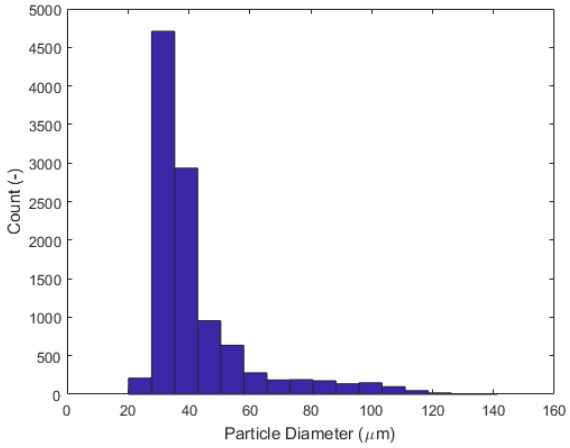

Fig. 7. Droplet size distribution immediately below ultrasonic nozzle.

4.2. Trajectory of Spray Particles Above the Substrate

Figure 8 shows the flow path of the vapor particles from the ultrasonic nozzle. The flow above the substrate makes a 90-degree turn, but some spray particles cannot follow the flow and are deposited on the surface., which could be due to the Wall effect or initial development of shear layer within the multiphase flow. As the turbulent eddies developed would compromise the surface of deposited electrolyte, causing unnecessary porosities and defects. The vorticial structure shown is a result of that 90-degree turn being made above the substrate. On the right-side of Figure 9, the circular flow path is plainly visible, whereas on the left-side it is not.

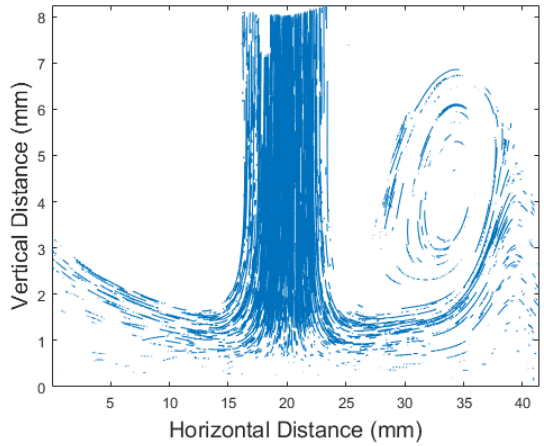

Fig. 8. Droplet particle trajectories above the substrate

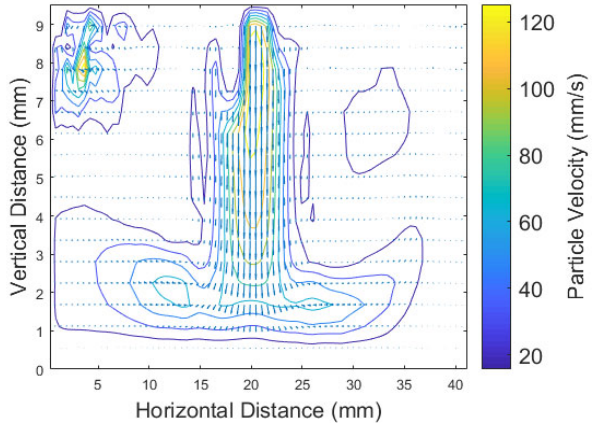

Fig. 9. Velocity map of droplet particles

Verification of the circular particle paths can be found in the velocity field shown in Figure 9. The maximum particle velocity was found to be 141 mm/s and takes place within the spray flow directly out of the nozzle. An average velocity of 23.0 mm/s was calculated, with a standard deviation of 18.0 mm/s.

The quiver arrows represent velocity magnitude and direction, where a longer arrow means a larger magnitude. A contour plot of velocity magnitude is overlain to aid in visualization. The circular pattern on the right-side still clearly shows the vortical structure of the flow path. However, now a similar pattern is clearly visible on the left-side as well. This indicates that a larger subtler pattern than that on the right also exists on the left. This finding is important for the redesign of manufacturing processes or parameter tune-up. Because the turbulent jet with sprays possesses a series of eddies that determine the distribution of deposition droplets or particles and, eventually, deposition pattern.

5. Conclusion and Future Work

In this study, a cyclone separator was simulated and integrated into an experimental EFAUSP setup. DIH was used to measure the droplet distribution from a 130 kHz ultrasonic nozzle. DIH was also used to estimate the effectiveness the separator and investigated droplet behavior near the substrate surface, where flow path vortices were recorded. Overall, the proposed method successfully eliminated the largest ultrasonically generated droplets.

In future work, the deposited electrolyte will contain lithium-bis(trifluoromethane) sulfonimide (LiTFSI) and an SiO_2 gradient with increasing SiO_2 concretion towards the anode. The samples will undergo electrochemical impedance spectroscopy, micro-indentation testing, and 3-point bending tests via a Dynamic Mechanical Analyzer. On the other hand, basic mechanisms on lithium dendrite growth need to be further researched to provide general guidelines for electrolyte design [56-59]. Last but not least, further study is needed to optimize and improve the efficiency of the fabrication approach for improved electrochemical performance.

Acknowledgements

This material is based upon work supported by the National Science Foundation under Award #1840732, the KU Research GO awards, KS NASA ESPCoR program, KU SOE RISe and KU General Research Funds. Any opinions, conclusions or recommendations expressed are those of the authors and do not necessarily reflect views of the sponsoring agencies. Any opinions, findings, and conclusions or recommendations expressed in this material are those of the author(s) and do not necessarily reflect the views of the sponsors. The authors appreciate the support from their sponsors.

References

[1] Fenton DE, Parker JM, Wright PV. Complexes of alkali metal ions with poly(ethylene oxide). Polymer. 1973;14:589.
[2] Christensen J, Albertus P, Sanchez-Carrera RS, Lohmann T, Kozinsky B, Liedtke R, et al. A Critical Review of Li / Air Batteries. Journal of The Electrochemical Society. 2012;159.
[3] Balaish M, Kraytsberg A, Ein-Eli Y. A critical review on lithium-air battery electrolytes. Phys Chem Chem Phys. 2014;16:2801-22.
[4] Oleg S, Vikram P, Abhishek K, Chayanit C, Venkatasubramanian V. Quantifying the promise of 'beyond' Li–ion batteries. Translational Materials Research. 2015;2:045002.
[5] Lu L, Han X, Li J, Hua J, Ouyang M. A review on the key issues for lithium-ion battery management in electric vehicles. Journal of Power Sources. 2013;226:272-88.
[6] Zhu J, Yang J, Zhou J, Zhang T, Li L, Wang J, et al. A stable organic–inorganic hybrid layer protected lithium metal anode for long-cycle lithium-oxygen batteries. Journal of Power Sources. 2017;366:265-9.

[7] Cheng X-B, Zhang R, Zhao C-Z, Zhang Q. Toward Safe Lithium Metal Anode in Rechargeable Batteries: A Review. Chemical Reviews. 2017;117:10403-73.
[8] Song YL, Tsai SC, Chen CY, Tseng TK, Tsai CS, Chen JW, et al. Ultrasonic Spray Pyrolysis for Synthesis of Spherical Zirconia Particles. Journal of the American Ceramic Society. 2004;87:1864-71.
[9] Zhu Y, Choi SH, Fan X, Shin J, Ma Z, Zachariah MR, et al. Recent Progress on Spray Pyrolysis for High Performance Electrode Materials in Lithium and Sodium Rechargeable Batteries. Advanced Energy Materials. 2017;7.
[10] Zhang J, Seyedin S, Gu Z, Salim N, Wang X, Razal JM. Liquid Crystals of Graphene Oxide: A Route Towards Solution‐Based Processing and Applications. Particle & Particle Systems Characterization. 2017;34:1600396.
[11] Park MS, Ma SB, Lee DJ, Im D, Doo S-G, Yamamoto O. A Highly Reversible Lithium Metal Anode. Scientific Reports. 2014;4:3815.
[12] Abdullah T, Liu L. Peak Power Optimization of Solid Oxide Fuel Cells with Particle Size and Porosity Grading. ECS Transactions. 2014;61:33-46.
[13] Liu L, Guan P, Liu C. Experimental and Simulation Investigations of Porosity Graded Cathodes in Mitigating Battery Degradation of High Voltage Lithium-Ion Batteries. Journal of The Electrochemical Society. 2017;164:A3163-A73.
[14] Liu L, Guan P. Phase-Field Modeling of Solid Electrolyte Interphase (SEI) Evolution: Considering Cracking and Dissolution during Battery Cycling. ECS Transactions. 2019;89:101-11.
[15] Zewde BW, Carbone L, Greenbaum S, Hassoun J. A novel polymer electrolyte membrane for application in solid state lithium metal battery. Solid State Ionics. 2018;317:97-102.
[16] Varzi A, Raccichini R, Passerini S, Scrosati B. Challenges and prospects of the role of solid electrolytes in the revitalization of lithium metal batteries. Journal of Materials Chemistry A. 2016;4:17251-9.
[17] Wan J, Xie J, Mackanic DG, Burke W, Bao Z, Cui Y. Status, promises, and challenges of nanocomposite solid-state electrolytes for safe and high performance lithium batteries. Materials Today Nano. 2018;4:1-16.
[18] Agrawal RC, Pandey GP. Solid polymer electrolytes: materials designing and all-solid-state battery applications: an overview. Journal of Physics D: Applied Physics. 2008;41:223001.
[19] Long L, Wang S, Xiao M, Meng Y. Polymer electrolytes for lithium polymer batteries. Journal of Materials Chemistry A. 2016;4:10038-69.
[20] Deng Y, Li J, Li T, Zhang J, Yang F, Yuan C. Life cycle assessment of high capacity molybdenum disulfide lithium-ion battery for electric vehicles. Energy. 2017;123:77-88.
[21] Li J, Liang X, Liou F, Park J. Macro-/Micro-Controlled 3D Lithium-Ion Batteries via Additive Manufacturing and Electric Field Processing. Scientific Reports. 2018;8:1846.
[22] Liu S, Wang H, Imanishi N, Zhang T, Hirano A, Takeda Y, et al. Effect of co-doping nano-silica filler and N-methyl-N-propylpiperidinium bis(trifluoromethanesulfonyl)imide into polymer electrolyte on Li dendrite formation in Li/poly(ethylene oxide)-Li(CF3SO2)2N/Li. Journal of Power Sources. 2011;196:7681-6.
[23] Glynos E, Papoutsakis L, Pan W, Giannelis EP, Nega AD, Mygiakis E, et al. Nanostructured Polymer Particles as Additives for High Conductivity, High Modulus Solid Polymer Electrolytes. Macromolecules. 2017;50:4699-706.
[24] Zhao Q, Chen P, Li S, Liu X, Archer LA. Solid-state polymer electrolytes stabilized by task-specific salt additives. Journal of Materials Chemistry A. 2019;7:7823-30.
[25] Khurana R, Schaefer JL, Archer LA, Coates GW. Suppression of Lithium Dendrite Growth Using Cross-Linked Polyethylene/Poly(ethylene oxide) Electrolytes: A New Approach for Practical Lithium-Metal Polymer Batteries. Journal of the American Chemical Society. 2014;136:7395-402.
[26] Manuel Stephan A, Nahm KS. Review on composite polymer electrolytes for lithium batteries. Polymer. 2006;47:5952-64.
[27] Kim J-W, Ji K-S, Lee J-P, Park J-W. Electrochemical characteristics of two types of PEO-based composite electrolyte with functional SiO2. Journal of Power Sources. 2003;119-121:415-21.
[28] Zhang W, Tu Z, Qian J, Choudhury S, Archer LA, Lu Y. Design Principles of Functional Polymer Separators for High-Energy, Metal-Based Batteries. Small. 2018;14:1703001.
[29] Ding L, Zhang A, Li W, Bai H, Li L. Multi-length scale porous polymer films from hypercrosslinked breath figure arrays. Journal of Colloid and Interface Science. 2016;461:179-84.
[30] Li H, Li M, Siyal SH, Zhu M, Lan J-L, Sui G, et al. A sandwich structure polymer/polymer-ceramics/polymer gel electrolytes for the safe, stable cycling of lithium metal batteries. Journal of Membrane Science. 2018;555:169-76.
[31] Lee J-G, Joshi BN, Lee J-H, Kim T-G, Kim D-Y, Al-Deyab SS, et al. Stable High-Capacity Lithium Ion Battery Anodes Produced by Supersonic Spray Deposition of Hematite Nanoparticles and Self-Healing Reduced Graphene Oxide. Electrochimica Acta. 2017;228:604-10.
[32] Djenadic R, Botros M, Benel C, Clemens O, Indris S, Choudhary A, et al. Nebulized spray pyrolysis of Al-doped Li7La3Zr2O12 solid electrolyte for battery applications. Solid State Ionics. 2014;263:49-56.
[33] Mezhericher M, Nunes JK, Guzowski JJ, Stone HA. Aerosol-assisted synthesis of submicron particles at room temperature using ultra-fine liquid atomization. Chemical Engineering Journal. 2018;346:606-20.
[34] Lee SM, Choi SH, Lee J-K, Kang YC. Electrochemical properties of graphene-MnO composite and hollow-structured MnO powders prepared by a simple one-pot spray pyrolysis process. Electrochimica Acta. 2014;132:441-7.
[35] Chen C, Kelder EM, van der Put PJJM, Schoonman J. Morphology control of thin LiCoO2 films fabricated using the electrostatic spray deposition (ESD) technique. Journal of Materials Chemistry. 1996;6:765-71.
[36] Sabnis SM, Bhadane PA, kulkarni PG. Process flow of spray pyrolysis technique. IOSR Journal of Applied Physics. 2013;4:07-11.
[37] Asim N, Ahmadi S, Alghoul MA, Hammadi FY, Saeedfar K, Sopian K. Research and Development Aspects on Chemical Preparation Techniques of Photoanodes for Dye Sensitized Solar Cells. International Journal of Photoenergy. 2014;2014:1-21.
[38] GAUCKLER DPLJ. Thin Film Deposition Using Spray Pyrolysis. Journal of Electroceramics. 2004;14:103-11.
[39] Ukoba KO, Eloka-Eboka AC, Inambao FL. Review of nanostructured NiO thin film deposition using the spray pyrolysis technique. Renewable and Sustainable Energy Reviews. 2018;82:2900-15.
[40] Li J, Wu R, Jing Z, Yan L, Zha F, Lei Z. One-Step Spray-Coating Process for the Fabrication of Colorful Superhydrophobic Coatings with Excellent Corrosion Resistance. Langmuir. 2015;31:10702-7.
[41] Tsai SC, Luu P, Childs P, Teshome A, Tsai CS. The role of capillary waves in two-fluid atomization. Physics of Fluids. 1997;9:2909-18.
[42] Slegers S, Linzas M, Drijkoningen J, D'Haen J, Reddy NK, Deferme W. Surface Roughness Reduction of Additive Manufactured Products by Applying a Functional Coating Using Ultrasonic Spray Coating. Coatings. 2017;7:208.
[43] Liu S, Imanishi N, Zhang T, Hirano A, Takeda Y, Yamamoto O, et al. Effect of nano-silica filler in polymer electrolyte on Li dendrite formation in Li/poly(ethylene oxide)–Li(CF3SO2)2N/Li. Journal of Power Sources. 2010;195:6847-53.
[44] Lang RJ. Ultrasonic Atomization of Liquids. The Journal of the Acoustical Society of America. 1962;34:6-8.
[45] Blake AJ, Kohlmeyer RR, Hardin JO, Carmona EA, Maruyama B, Berrigan JD, et al. 3D Printable Ceramic–Polymer Electrolytes for Flexible High-Performance Li-Ion Batteries with Enhanced Thermal Stability. Advanced Energy Materials. 2017;7:1602920.
[46] Ketut C, Dwinanto, Attegar. Optimization high vortex finder of cyclone separator with computational fluids dynamics simulation2017.
[47] Gronowska MA. Specification of forces in rotational separator. 2012;59:49.
[48] Hoffmann AC. Gas Cyclones and Swirl Tubes : Principles, Design, and Operation. 2nd ed.. ed. Berlin
New York: Berlin
New York : Springer; 2007.
[49] Sun X, Kim S, Yang SD, Kim HS, Yoon JY. Multi-objective optimization of a Stairmand cyclone separator using response surface methodology and computational fluid dynamics. Powder Technology. 2017;320:51-65.
[50] Strob R, Dobrowolski A, Pieloth D, Schaldach G, Wiggers H, Walzel P, et al. Preparation and characterization of spray-dried submicron particles

for pharmaceutical application. Advanced Powder Technology. 2018;29:2920-7.
[51] Yang Y, Li J, Chen D, Zhao J. Spray Drying-Assisted Synthesis of Li3VO4/C/CNTs Composites for High-Performance Lithium Ion Battery Anodes. Journal of The Electrochemical Society. 2017;164:A6001-A6.
[52] M. Durango-Cogollo, J. Garcia-Bravo, B. Newell and A. Gonzalez-Mancera. CFD Modeling of Hydrocyclones—A Study of Efficiency of Hydrodynamic Reservoirs. Fluids. 2020;5:118-137.
[53] Katz J, Sheng J. Applications of Holography in Fluid Mechanics and Particle Dynamics. Annual Review of Fluid Mechanics. 2010;42:531-55.
[54] Shao S, Li C, Hong J. A hybrid image processing method for measuring 3D bubble distribution using digital inline holography. Chemical Engineering Science. 2019;207:929-41.
[55] Kumar SS, Li C, Christen CE, Hogan CJ, Fredericks SA, Hong J. Automated droplet size distribution measurements using digital inline holography. Journal of Aerosol Science. 2019;137:105442.
[56] Qian D, Liu X, Rou R, Wen Z, Zhou W, Liu L. Quantitative analysis of the inhibition effect of rising temperature and pulse charging on Lithium dendrite growth. Journal of Energy Storage. 2022;49:104137.
[57] Jiang K, Liu X, Yi X, Lou G, Wen Z, Liu L. Modeling of solid-state lithium-oxygen battery with porous $Li_{1.3}Al_{0.3}Ti_{1.7}(PO_4)_3$-based cathode. . Journal of Energy Storage. 2022;45:103747.
[58] Jiang K, Liu X, Lou G, Wen Z, Zhou W, Liu L. Parameter sensitivity analysis and cathode structure optimization of a non-aqueous Li–O2 battery model. Journal of Power Sources. 2020;451:227821.
[59] Mu W Liu X, Wen Z, Liu L. Numerical simulation of the factors affecting the growth of lithium dendrites. Journal of Energy Storage. 2019;26:1.